Cell Metabolism
Article

Endothelin-3 Expression in the Subfornical Organ Enhances the Sensitivity of Na_x, the Brain Sodium-Level Sensor, to Suppress Salt Intake

Takeshi Y. Hiyama,[1,3] Masahide Yoshida,[1,4] Masahito Matsumoto,[1] Ryoko Suzuki,[1] Takashi Matsuda,[1,3] Eiji Watanabe,[2,3] and Masaharu Noda[1,3,*]
[1]Division of Molecular Neurobiology
[2]Laboratory of Neurophysiology
National Institute for Basic Biology, Okazaki, Aichi 444-8787, Japan
[3]School of Life Science, The Graduate University for Advanced Studies, Okazaki, Aichi 444-8787, Japan
[4]Present address: Division of Brain and Neurophysiology, Department of Physiology, Jichi Medical University, Shimotsuke, Tochigi 329-0498, Japan
*Correspondence: madon@nibb.ac.jp
http://dx.doi.org/10.1016/j.cmet.2013.02.018

SUMMARY

Salt homeostasis is essential to survival, but brain mechanisms for salt-intake control have not been fully elucidated. Here, we found that the sensitivity of Na_x channels to $[Na^+]_o$ is dose-dependently enhanced by endothelin-3 (ET-3). Na_x channels began to open when $[Na^+]_o$ exceeded ~150 mM without ET-3, but opened fully at a physiological $[Na^+]_o$ (135–145 mM) with 1 nM ET-3. Importantly, ET-3 was expressed in the subfornical organ (SFO) along with Na_x, and the level was robustly increased by dehydration. Pharmacological experiments revealed that endothelin receptor B (ET_BR) signaling is involved in this modulation of Na_x gating through protein kinase C and ERK1/2 activation. ET_BR agonists increased the firing rate of GABAergic neurons via lactate in the SFO, and an ET_BR antagonist attenuated salt aversion during dehydration. These results indicate that ET-3 expression in the SFO is tightly coupled with body-fluid homeostasis through modulation of the $[Na^+]_o$ sensitivity of Na_x.

INTRODUCTION

As the major electrolyte of the extracellular fluid, sodium (Na) plays a fundamental role in maintaining the volume and composition of every fluid compartment in the body (Fitzsimons, 1998). As such, the amount of Na in body fluids must be tightly regulated to ensure optimal performance of numerous physiological processes based on the ion concentration across cell membranes, including neuronal excitability, substance transport, glomerular filtration and renal excretion of aqueous waste, and the control of extracellular volume and blood pressure (Daniels and Fluharty, 2004). Thus, Na is a key component of many mammalian physiological functions. Disorders of Na homeostasis induce severe consequences, such as exaggerated vascular reactivity, hypertension, or circulatory collapse (Lin et al., 2005).

Na_x, structurally classified as a family of voltage-gated Na channels (Goldin et al., 2000), is a Na^+ concentration ($[Na^+]$)-sensitive channel with an apparent threshold value of ~150 mM for extracellular $[Na^+]$ ($[Na^+]_o$) in vitro (Hiyama et al., 2002; Noda, 2006). Na_x is predominantly expressed in glial cells (ependymal cells and astrocytes) of the circumventricular organs (CVOs) in the brain, including the subfornical organ (SFO) and organum vasculosum of the lamina terminalis (Watanabe et al., 2000, 2006). *Na_x*-knockout (*Na_x*-KO) mice do not stop ingesting salt even when dehydrated (Watanabe et al., 2000). This behavioral anomaly of *Na_x*-KO mice is reversed by site-directed expression of the *Na_x* gene in the SFO (Hiyama et al., 2004). Na_x thus appears to be the brain's $[Na^+]_o$ sensor involved in body-fluid homeostasis (Noda, 2007).

We subsequently revealed that Na_x in glial cells stably interacts with Na^+/K^+-ATPase to assist its activation (Shimizu et al., 2007). Because activation of Na^+/K^+-ATPase consumes ATP, Na^+ influx via Na_x leads to an increase of glucose uptake and the activation of anaerobic glucose metabolism of Na_x-positive glial cells (Shimizu et al., 2007). Consequently, the release of lactate from the glial cells is enhanced, and this lactate functions as a gliotransmitter to stimulate GABAergic neurons surrounded by the glial cells in the SFO (Shimizu et al., 2007). The supply of lactate from glial cells to neurons appears to be central to the control of salt-intake behavior in dehydrated animals (Shimizu et al., 2007).

As aforementioned, Na_x showed a threshold value of ~150 mM for $[Na^+]_o$ in vitro. However, we should note here that $[Na^+]$ in serum and cerebrospinal fluid (CSF) is strictly controlled at 135–145 mM in mammals, including humans (Peruzzo et al., 2010), suggesting that the brain sensor(s) can detect an increase in $[Na^+]$ in this range to strictly maintain the physiological level. We therefore presumed that the threshold value of Na_x for $[Na^+]_o$ must be modulated in vivo by some mechanism. The SFO has been shown to harbor not only sensors for ionic conditions in body fluids but also receptors for a variety of regulatory peptides (Mendelsohn et al., 1984; Saavedra et al., 1986; Barth et al., 2004). Recently, a transcriptome analysis using a microarray revealed that ET_BR, a receptor for

endothelins (ETs), is extremely highly expressed in the rat SFO (Hindmarch et al., 2008). ET_BR is predominantly expressed in glial cells in the brain (Hori et al., 1992). Furthermore, ET peptides and their receptors are intimately involved in the physiological control of systemic blood pressure and Na homeostasis (Kohan et al., 2011). It is thus tempting to speculate that ET is involved in signaling mechanisms mediated by sensor molecules such as Na_x in the SFO.

ETs are 21-amino-acid peptides originally cloned from aortic endothelial cells (Kedzierski and Yanagisawa, 2001). Three structurally related peptides, ET-1, ET-2, and ET-3, have been identified (Kedzierski and Yanagisawa, 2001). In mammals, ETs generate their biological effects via the activation of two receptor subtypes: ET receptor type A (ET_AR) and ET receptor type B (ET_BR). The rank order of affinity of ETs for ET_AR is ET-1 > ET-2 >> ET-3 at subnanomolar to micromolar concentrations, whereas ET_BR binds to ETs with approximately equal affinity in the subnanomolar range (Kedzierski and Yanagisawa, 2001; Arai et al., 1990; Sakurai et al., 1990). Both ET_AR and ET_BR are seven-transmembrane proteins coupled to G proteins, leading to multiple second messenger systems (Sokolovsky, 1995).

In the present study, we found that ET-3 shifts the $[Na^+]_o$ dependency of Na_x activation to the lower-concentration side in a dose-dependent manner, and thereby gated Na_x even when $[Na^+]_o$ was in the physiological range. ET_BR signaling promoted activation of Na_x through protein kinase C (PKC) pathways leading to extracellular signal-regulated kinase 1/2 (ERK1/2) activation. Importantly, expression of ET-3 in the SFO was time-dependently enhanced during dehydration. Moreover, a specific blocker of ET_BR BQ788 attenuated the salt-aversive behavior in wild-type (WT) mice induced by dehydration. These results strongly indicate that regulated expression of ET-3 in the SFO is involved in the control of salt-intake behavior through improvement of the $[Na^+]_o$ sensitivity of Na_x in vivo.

RESULTS

ET_BR Is Expressed in Na_x-Positive Glial Cells in the SFO

We first attempted to identify cells expressing *ET_AR* and *ET_BR* messenger RNA (mRNA) in the SFO in hydrated mice using in situ hybridization. *ET_BR* but not *ET_AR* mRNA expression was detected in ependymal cells facing the dorsal third ventricle and inside cells of the SFO (Figure 1A). Because the expression pattern of *ET_BR* mRNA was highly similar to that of *Na_x* mRNA (see Shimizu et al., 2007), we examined whether Na_x-positive glial cells express ET_BR in the SFO. Double immunostaining of the SFO (Figure 1B) and dissociated SFO cells (Figure 1C) verified the coexpression of Na_x and ET_BR at the cellular level.

ET-3 and Endothelin-Converting Enzymes Are Expressed in the SFO

We then investigated the expression of mRNAs for ETs (ET-1, ET-2, and ET-3) in the SFO by in situ hybridization under hydrated conditions (Figure 1D). *ET-3* but not *ET-1* or *ET-2* mRNA was detected in ependymal cells of the SFO facing the dorsal third ventricle and in some cells inside the SFO. Endothelin-converting enzymes (Ece1 and Ece2), proteases responsible for the conversion of inactive ET precursors (big endothelin) to bioactive mature forms (Kedzierski and Yanagisawa, 2001), were also expressed in the SFO in a similar fashion (Figure 1E). Sense probes gave no signals in in situ hybridization (data not shown).

ET-3 Opens Na_x Channels at 145 mM $[Na^+]_o$ via ET_BR

Because Na_x and ET_BR colocalized at the cellular level, we theorized that the gating (or signaling) of Na_x is directly (or indirectly) modulated by ET signaling via ET_BR. To test this possibility, we examined the effect of ET-3 on Na_x activation using cells dissociated from the SFO by intracellular Na^+ imaging. Surprisingly, ET-3 (0.1–10 nM) dose-dependently induced Na^+ influx in a subset of the SFO cells from WT mice in a 145 mM $[Na^+]$ solution, and these responsive cells were all positive for Na_x (Figures 1F–1H; WT; ET-3, 0.1, 0.3, 1, or 10; BQ788 −). In contrast, cells from *Na_x*-KO mice did not respond to ET-3 at all (Figures 1F–1H; KO; ET-3, 10; BQ788 −). Expectedly, the responses by ET-3 observed in WT cells were completely blocked by an ET_BR antagonist, BQ788 (Figures 1F–1H; WT; ET-3, 10; BQ788 +). Of note, angiotensin II (Ang II; 100 nM) did not induce Na^+ influx in the SFO cells under the same condition (Figures 1G and 1H; WT; Ang II).

We confirmed these results electrophysiologically by the perforated patch-clamp method using β-escin (Fan and Palade, 1998). Addition of ET-3 (1 nM) to the perfusate ($[Na^+]_o$ = 140 mM) resulted in a gradual increase of whole-cell Na^+ currents in Na_x-positive cells, reaching a plateau in 15 min (Figure 2A, WT; n = 8). The ET-dependent current reversed at a potential close to the Na^+ equilibrium potential (E_{Na}) (Figure 2B; ~80 mV, E_{Na} = 81.0 mV for $[Na^+]_o$ = 140 mM). The reversal potentials shifted in the negative direction as $[Na^+]_o$ was decreased, and they agreed well with values predicted by the Nernst equation for Na^+ permeability (data not shown). Of note, the current was not observed at all in SFO cells of *Na_x*-KO mice (Figure 2A, KO; n = 8). Taken together, these data indicate that the inward current induced by ET-3 is Na^+ current mediated by Na_x channels.

The plateau amplitude of the current was dependent on the concentration of ET-3 ([ET-3]) and reached a peak at ~10 nM when $[Na^+]_o$ was 140 mM (Figures 2C and 2D; ET-3 concentration that elicits half-maximal response, $C_{1/2}$, was 0.52 nM). The current response by ET-3 was completely blocked by preincubation with 100 nM BQ788 (data not shown). As was expected, the maximal level of the current density induced by ET-3 (~1.5 pA/pF at 10 nM ET-3; Figure 2D) was equal to that induced by an increase of $[Na^+]_o$ (~1.5 pA/pF at 170 mM $[Na^+]_o$; Figure 2D).

ET-3 Signaling Shifts the $[Na^+]_o$ Sensitivity for Na_x Gating toward the Lower Side

When the "high Na^+ solution" ($[Na^+]_o$ = 170 mM) was applied to the SFO cells derived from WT mice, inward currents (the maximum current) were observed in Na_x-positive cells (Figure 2E, i). It was not inactivated under the high-Na^+ solution conditions, but it disappeared rapidly when $[Na^+]_o$ was set back to the basal level ($[Na^+]_o$ = 140 mM). These current properties observed in Na_x-positive glial cells in the SFO are thus similar to those previously reported in Na_x-positive DRG neurons, including noninactivating currents with a linear I-V relationship (Hiyama et al., 2002).

After the amplitude of ET-3-induced current almost reached the maximum level (under the condition that Na_x channels

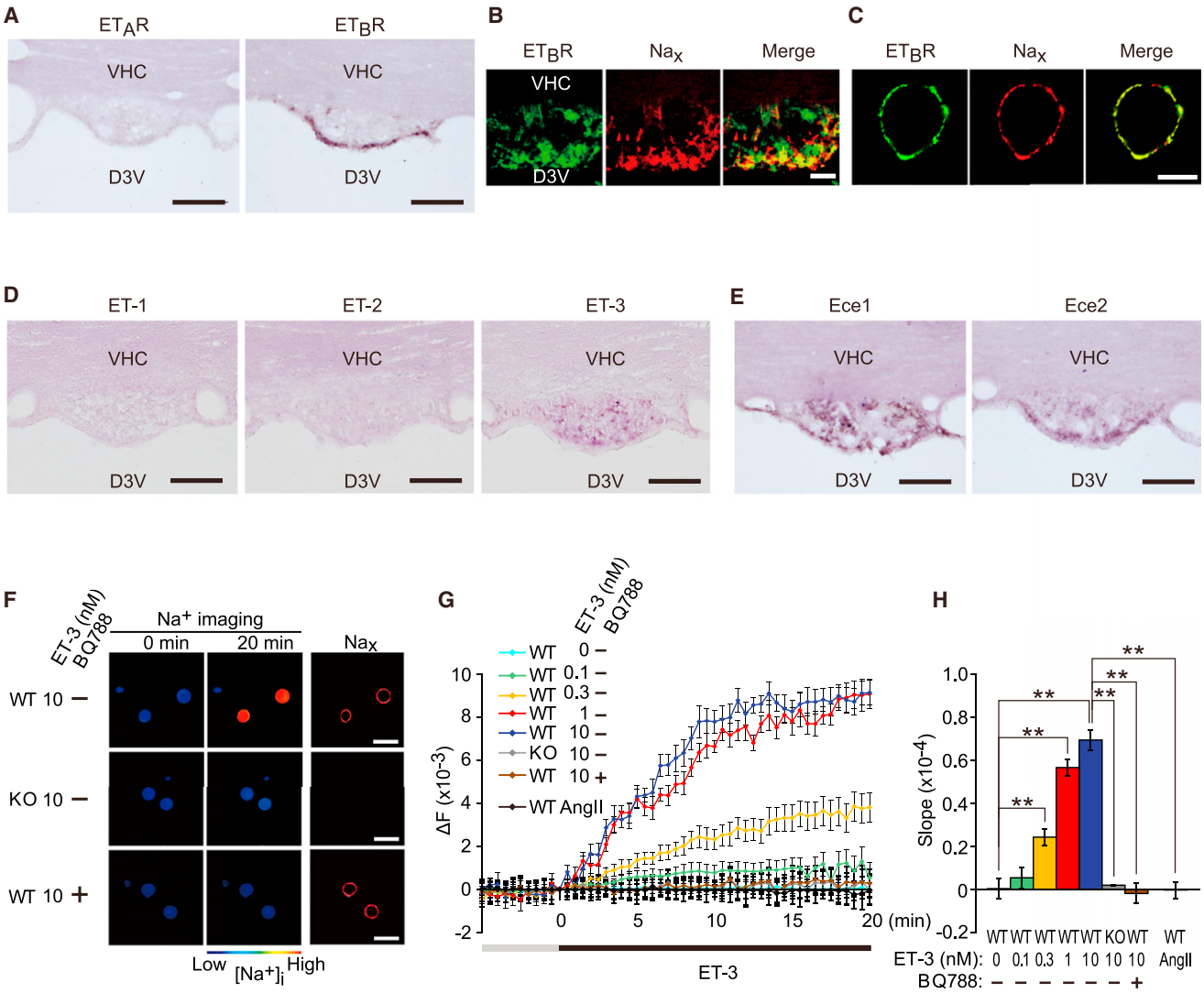

Figure 1. ET-3 Induces Na^+ Influx in Na_x-Positive Cells in the SFO via ET_BR

(A) In situ hybridization for *ET_AR* and *ET_BR* mRNAs on coronal sections of the SFO. ET_BR signals were detected in ependymal cells facing the D3V and astrocytes inside the SFO. Scale bars, 100 μm. VHC, ventral hippocampal commissure; D3V, dorsal third ventricle.

(B) Double immunohistochemical detection of ET_BR and Na_x. Scale bar, 50 μm.

(C) Double immunocytochemical detection of ET_BR and Na_x in a dissociated SFO cells. Colocalization of ET_BR and Na_x was observed in the plasma membrane. Na_x-positive cells are large round cells, which we previously identified as glial cells (ependymal cells and astrocytes; Shimizu et al., 2007). Scale bar, 10 μm.

(D) In situ hybridization for *ET-1*, *ET-2*, and *ET-3* mRNAs. Neither *ET-1* nor *ET-2* mRNA was detected. *ET-3* mRNA was detected in ependymal cells and cells inside the SFO. Scale bars, 100 μm.

(E) In situ hybridization of *Ece1* and *Ece2*. *Ece1* and *Ece2* mRNA were detected in ependymal cells and cells inside the SFO. Scale bars, 100 μm.

(F) Representative images of Na^+ influx in SFO cells obtained from WT and *Na_x*-KO (KO) mice. The pseudocolor images indicate the intracellular Na^+ concentration ($[Na^+]_i$) at 0 and 20 min after the start of the application of 10 nM ET-3. In the experiments on ET_BR inhibition, BQ788 (100 nM) was added to the extracellular solution 20 min before the start of the experiments. Large round glial cells showed the response. Scale bars, 30 μm.

(G) Time course of the cellular Na^+ imaging. The ordinate indicates the fluorescence ratio (ΔF; 340/380 nm) representing $[Na^+]_i$. The fluorescence ratio at 0 min was set as zero points on the ordinate. The extracellular fluid ($[Na^+]_o$ = 145 mM) was changed to that containing ET-3 or angiotensin II at 0 min. Data were collected from large round cells, which were identified as Na_x-positive glial cells by immunostaining. Data are mean ±SEM (n = 20 for each). BQ788 −, vehicle; BQ788 +, 100 nM BQ788; Ang II, 100 nM angiotensin II.

(H) Summary of the rate of increase in $[Na^+]_i$ (Slope) in (G). The ordinate indicates the slope of the change in the fluorescence ratio between 3 and 8 min, where the graph shows good linearity. **$p < 0.01$, two-tailed Student's t test; data are mean ±SEM (n = 20 for each).

were almost open by ET-3), the high-Na^+ solution was applied further to estimate the additional current amount produced $[Na^+]_o$ dependently (Figure 2E, ii). The additional current response was expectedly very small, and the total current amplitude from the basal level (indicated with a dotted line in blue) was almost the same as that at (i). This is consistent with the notion

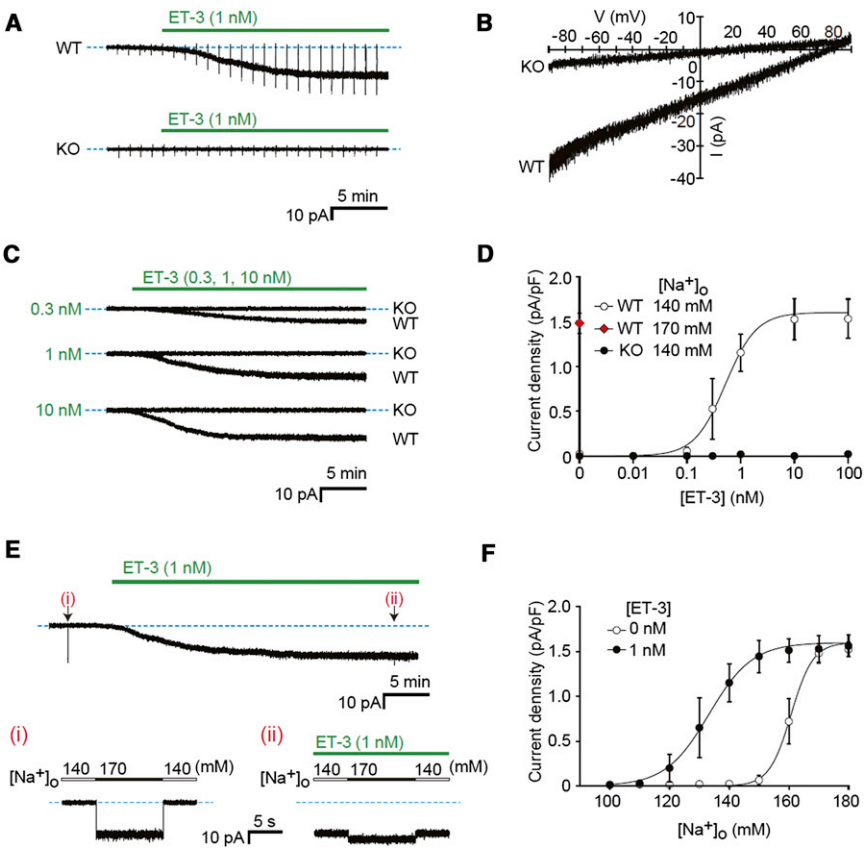

Figure 2. ET-3 Signaling Shifts the $[Na^+]_o$ Dependency of Na_x Activation to the Lower Side

(A) Representative whole-cell current responses in the large round glial cells obtained from the SFO of WT and *Na_x*-KO (KO) mice on application of 1 nM ET-3. Current deflections represent current responses to 1 s voltage ramps that were applied every 1 min (from −90 to +90 mV). The holding potential was set at −45 mV. The currents were recorded with patch pipettes filled with a Cs^+-based pipette solution containing tetraethylammonium to block K^+ currents. The dotted lines represent the basal level without ET-3 application.

(B) Representative ramp currents of the WT and KO cells obtained 15 min after the start of the ET-3 application.

(C) Representative whole-cell current responses in the WT and KO cells on application of 0.3, 1, or 10 nM ET-3, under the 140 mM $[Na^+]_o$ condition. The dotted lines represent the basal level without ET-3.

(D) Relationships between the current density (current amplitude/cell capacitance) and [ET-3] in the SFO cells obtained from WT and KO mice. The current amplitude from the basal level was measured 20 min after the start of the ET-3 application. The abscissa is shown in the logarithmic scale. $[Na^+]_o$ at the half-maximal response ($C_{1/2}$) was determined by curve fitting; the curve is shown with a solid line. Data are mean ±SEM (n = 6 for each).

(E) A representative whole-cell current response of a SFO cell obtained from WT mice on application of hypertonic Na^+. The transient application of hypertonic Na^+ (170 mM) was performed at the time points indicated by arrows, 5 min before (i) and 30 min after (ii) the start of the ET-3 application (1 nM). The dotted lines represent the basal level under the 140 mM $[Na^+]_o$ condition without ET-3. The currents induced by an increase in $[Na^+]_o$ (30 mM) at the time points (i) and (ii) are magnified below.

(F) Relationships between the current density and $[Na^+]_o$ in the presence or absence of 1 nM ET-3. The current amplitudes from the basal level were measured and plotted. For comparisons, the current changes due to the shift of the E_{Na} were compensated. Data are mean ±SEM (n = 6 for each point). The $C_{1/2}$ values were determined after curves fitting (solid lines).

that both $[Na^+]_o$- and [ET]-dependent currents are mediated by Na_x channels.

We further examined the relationship between $[Na^+]_o$- and [ET]-dependent responses. The $[Na^+]_o$-dependent response reached a maximum at ~170 mM without ET-3; here, $C_{1/2}$ was 161 mM (Figure 2F; [ET-3] = 0 nM). This $C_{1/2}$ value matched well with our previous estimation (157 mM) obtained using Na^+-imaging techniques (Hiyama et al., 2002). When 1 nM ET-3 was applied, the response curve of $[Na^+]_o$ dependency shifted to the lower side; the $C_{1/2}$ value was shifted to 133 mM (Figure 2F; [ET-3] = 1 nM). Intriguingly, the slope of $[Na^+]_o$-dependence curve at 1 nM ET-3 was less steep than that without ET-3, indicating that ET-3 signaling makes Na_x channels sensitive in a wider range of $[Na^+]_o$ (Figure 2F).

Modulation of Na_x Gating by ET-3 in SFO Cells Was Reproduced in C6 Cells Expressing both Na_x and ET_BR

We next tested by Na^+ imaging whether the Na_x response observed in the SFO cells is reproducible in C6M16 cells (Shimizu et al., 2007), in which the expression of Na_x channels can be induced by the Tet-off system (Figure 3A). We confirmed beforehand that ET_BR is expressed in C6M16 cells (Figures 3B and 3C). In the Na_x-positive C6M16 cells, ET-3 (10 nM) at 145 mM $[Na^+]_o$ induced Na^+ influx with a similar time course as the SFO cells, and the response was blocked by the ET_BR antagonist BQ788 (Figure S1 available online). Consistently, the ET_BR-specific agonist IRL1620 induced Na^+ influx in a dose-dependent manner with a saturated response at 100 nM (Figure 3D). Here, it should be noted that ET_BR activation did not affect the cell-surface expression of Na_x in Na_x-positive C6M16 cells (Figure S2).

The relationship between $[Na^+]_o$- and [ET]-dependent activation of Na_x was examined in depth using C6M16 cells by Na^+-imaging experiments. Without the ET_BR agonist IRL1620, the $[Na^+]_o$-dependent response reached a maximum at 170 mM; here, $C_{1/2}$ was estimated as 161 mM (Figure 3E; IRL, 0; BQ −). The $[Na^+]_o$-dependence curve did not significantly differ in the presence and absence of the ET_BR antagonist BQ788 (100 nM) (Figure 3E; compare IRL, 0; BQ + with IRL, 0; BQ −). When IRL1620 was applied at 50 nM, however, the $[Na^+]_o$ dependency of the response shifted to the lower side; $C_{1/2}$ was shifted to 146 mM (Figure 3E; IRL, 50; BQ −). When IRL1620 was applied at 100 nM, the $[Na^+]_o$-dependence curve further shifted toward a lower $[Na^+]_o$; $C_{1/2}$ was 132 mM (Figure 3E; IRL, 100; BQ −).

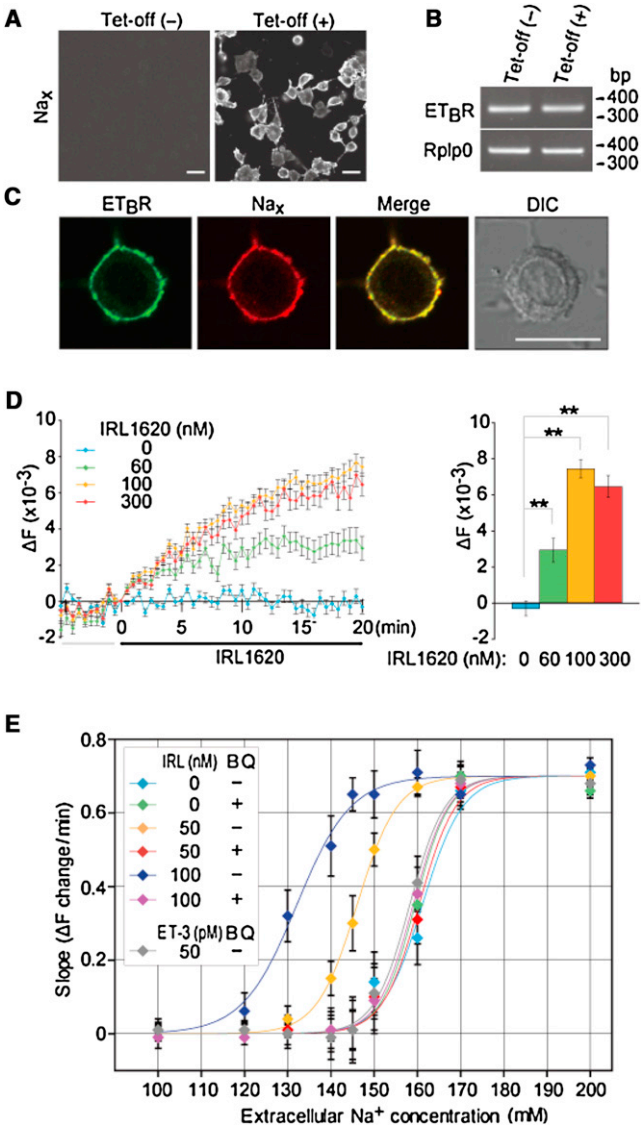

Figure 3. ET_BR Agonist Induces Na^+ Influx in a Cell Line Expressing Na_x and ET_BR

(A) Immunostaining for Na_x expressed in C6M16 cells. The Tet-off regulator induces the expression of Na_x. Scale bars, 25 μm.

(B) *ET_BR* mRNA expression in the C6M16 cells. Total RNA extracted from Na_x-negative [Tet-off (−)] and Na_x-positive [Tet-off (+)] C6M16 cells was subjected to RT-PCR. *Rplp0*, ribosomal protein large P0 used as a control.

(C) Immunostaining of ET_BR and Na_x in C6M16 cells. Scale bar, 20 μm. DIC, differential interference contrast image.

(D) Left: Intracellular Na^+ imaging with the ET_BR agonist IRL1620 at each dose in Na_x-positive C6M16 cells. Right: Summary of the fluorescence ratio (ΔF) at 20 min in the left panel. **p < 0.01, two-tailed Student's t test; data are mean ±SEM (n = 30 for each).

(E) Relationships between the rate of increase in $[Na^+]_i$ (Slope) and $[Na^+]_o$ at various concentrations of IRL1620 and ET-3 in the presence or absence of BQ788 (100 nM). The ordinate indicates the slope in the curve of the fluorescence ratio between 5 and 10 min. The values of $C_{1/2}$ were determined by curve fitting (solid lines). Data are mean ±SEM (n = 30 for each). BQ −, vehicle; BQ +, 100 nM BQ788. See also Figures S1 and S2.

BQ788 (100 nM) completely abrogated the shift of the curves by IRL1620 (Figure 3E; IRL, 50; BQ + and IRL, 100; BQ +). Because IRL1620 at 100 nM induced full activation of Na_x (see Figure 3D), the response curve at 100 nM IRL1620 indicates that an $[Na^+]_o$ of at least 100 mM is required for the activation of Na_x by ET_BR signaling (Figure 3E; IRL, 100; BQ −).

Of note, 50 pM ET-3 did not shift the curve at all (Figure 3E; ET-3, 50; BQ −). This suggests that it is unlikely that ET-3 from blood or CSF activates Na_x in the SFO (see below), even though the CVOs lack a blood-brain barrier.

Na_x Activation Is Mediated by PKC Pathways Leading to ERK1/2 Activation Downstream

The signaling from ET_BR is reportedly transduced via $G_{\alpha i}$- and $G_{\alpha q}$-dependent pathways (Rauh et al., 2008). $G_{\alpha i}$ directly activates Src, which leads to activation of Ras/Raf. Conversely, the $G_{\alpha q}$ pathway first activates PKC and then activates Src and Ras/Raf (Robin et al., 2002). Both pathways eventually converge to activate ERK1/2 downstream through mitogen-activated protein kinase/ERK kinase (MEK) (Figure 4A). We tested whether this is also the case for C6M16 cells. After stimulation with the ET_BR agonist IRL1620, we first examined ERK1/2 activation with an anti-phospho-ERK1/2 antibody using C6M16 cells expressing Na_x. The phosphorylation of ERK1/2 was time-dependently increased by IRL1620, peaking at 10 min (Figure 4B).

We then pharmacologically investigated which ET_BR signaling cascade is involved in the activation of Na_x. The ET_BR agonist-induced Na^+ influx was not affected by a $G_{\alpha i}$ inhibitor, pertussis toxin (PTX) (Figure 4C), suggesting that the pathway indicated by dotted lines in Figure 4A is not used in C6M16 cells. On the other hand, the Na^+ influx was reduced to the basal level by the addition of inhibitors for PKC (bisindolylmaleimide I), MEK (U0126), and ERK1/2 (FR180204), respectively, but only partially blocked by an inhibitor of Src, 4-amino-5-(4-chloro-phenyl)-7-(t-butyl)pyrazolo[3,4-d]pyrimidine (PP2) (Figure 4C). These results indicate that the activation of Na_x channels by ETs occurs downstream of $G_{\alpha q}$, but not $G_{\alpha i}$ and that ERK1/2 activation downstream of PKC is essential for the Na^+ influx (Figure 4A). Also, IRL1620-induced phosphorylation of ERK1/2 was not blocked by PTX, but was blocked by inhibitors for PKC, Src, and MEK, respectively (Figure S3, IRL1620).

ET-3 Stimulates Cellular Glucose Uptake

As the Na^+ influx via Na_x directly stimulates Na^+/K^+-ATPase activity to pump out intracellular Na^+ ions and leads to enhancement of cellular glucose uptake and glycolysis (Shimizu et al., 2007), we assessed glucose uptake using a fluorescent glucose derivative, 2-NBDG, using the native cells from the SFO (Figures 5A–5D). We found that there existed cellular populations that intensively took up 2-NBDG on the application of ET-3 (10 nM) among the WT mouse cells but not the *Na_x*-KO cells (Figures 5A, 5B, and 5D). Importantly, these active cells were all positive for Na_x (Figure 5A), and the glucose-uptake activity was inhibited by the Na^+/K^+-ATPase inhibitor ouabain (1 mM; Figures 5C and 5D). These results indicate that the activation of Na_x channels by ET_BR signaling stimulates glucose metabolism in Na_x-positive glial cells in the SFO. We further confirmed that Na_x-positive C6M16 cells also show enhancement of glucose uptake by the

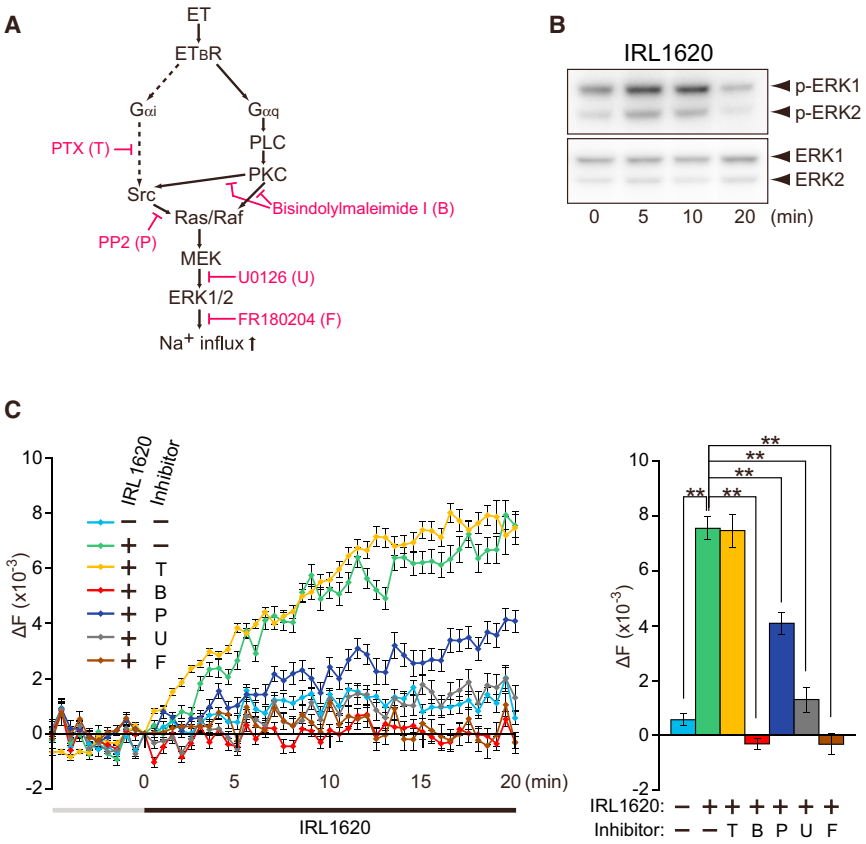

Figure 4. ET_BR Signaling Pathway Responsible for Na_x-Dependent Na^+ Influx

(A) Activation cascades of Na_x via the ET_BR receptor based on our experimental results. The kinase inhibitors used in the experiments are indicated in red. The pathway indicated by dotted lines was suggested not to work in the Na_x activation by ET_BR signaling (see Figures 4C, S3, and S4).

(B) ERK1/2 phosphorylation induced by 100 nM IRL1620. Extracts from Na_x-positive C6M16 cells were analyzed by western blotting using anti-phospho-ERK1/2 and anti-ERK1/2.

(C) Left: The effects of kinase inhibitors on Na^+-influx induced by 100 nM IRL1620 in Na_x-positive C6M16 cells. Inhibitors used are as follows: for $G_{\alpha i}$ (T; 100 ng/ml pertussis toxin), PKC (B; 3.75 μM bisindolylmaleimide I), Src (P; 10 μM PP2), MEK (U; 20 μM U0126), or ERK (F; 10 μM FR180204). The ordinate shows the fluorescence ratio (ΔF). The fluorescence ratio at 0 min was set as zero. Right: Summary of the fluorescence ratio at 20 min in the left panel. **$p < 0.01$, two-tailed Student's t test; data are mean ±SEM (n = 30 for each). See also Figure S3.

ET_BR agonist, and this enhancement was blocked by inhibitors for PKC, MEK, ERK, and Src, expectedly (Figure S4).

ET-3 Enhances Lactate Release in the SFO

Increased demand for glucose and stimulation of cellular anaerobic glycolysis by glial cells brings about the release of lactate (Shimizu et al., 2007). This suggests that Na_x activation by ET-3 also leads to the promotion of lactate release from Na_x-positive glial cells in the SFO. To confirm this view, we measured the amounts of lactate released from the SFO (Figure 5E). After the incubation of the SFO from WT mice with solutions containing 10 nM ET-3, the lactate concentration in the solutions was higher by more than 50% compared with that without ET-3 (Figure 5E; WT). This upregulation was completely abolished by 1 mM ouabain. In contrast, solutions containing ET-3 incubated with the SFO from *Na_x*-KO mice showed no such increases (Figure 5E; KO). These results indicate that anaerobic glycolysis was stimulated in Na_x-positive glial cells of the SFO by ET_BR signaling.

ET-3 Activates GABAergic Neurons in the SFO Na_x Dependently

Activation of Na_x in glial cells leads to an upregulation of the firing activity of GABAergic neurons in the SFO through secretion of lactate as a gliotransmitter (Shimizu et al., 2007). We next examined the effect of ET-3 on neuronal activities of GABAergic neurons in the SFO. We prepared acute slices containing the SFO from *GAD-GFP* and *GAD-GFP/Na_x*-KO mice (see Watanabe et al., 2006; GAD, glutamic acid decarboxylase), respectively, and examined the firing activity of GABAergic neurons using patch-clamp techniques in the cell-attached mode (Figures 5F and 5G). The GABAergic neurons carrying the fluorescence of GFP as a marker in the SFO of both WT and *Na_x*-KO mice showed spontaneous firing at a similar frequency under normal ($[Na^+]_o$ = 145 mM) conditions (~4 Hz; see Figure 5F, ET-3, 0). Upon addition of ET-3 (>0.3 nM) to the perfusate, the firing frequency in WT mice gradually increased. The average frequency during the 15–20 min after the ET-3 application showed concentration-dependent enhancement (Figure 5G; ET-3; 0.3, 1, 10), and ET-3 at 10 nM doubled the frequency (~8 Hz). This increase was not observed in *Na_x*-KO mice upon the addition of 10 nM ET-3 (Figures 5F and 5G, KO).

Lactate is known to be taken in by monocarboxylate transporters (MCTs) and fuel oxidative metabolism in neurons (Gladden, 2004). Therefore, we examined the effects of α-cyano-4-hydroxycinnamic acid (α-CHCA), an inhibitor of MCTs, on the firing rate, as we previously reported (Shimizu et al., 2007). The activation was abolished by preincubation not only with the ET_BR antagonist BQ788 but also with α-CHCA (Figure 5G), indicating that the activation of SFO GABAergic neurons by ET-3 was mediated by lactate signaling. These results with ET-3 were reproduced in experiments with the ET_BR agonist IRL1620 (Figure 5H). Upon addition of IRL1620 (100 nM) to the perfusate, the firing frequency of GABAergic neurons from WT mice, but not from *Na_x*-KO mice, gradually doubled. The enhancement of GABAergic activities was again abolished by preincubation with BQ788 or α-CHCA.

ET-3 Expression Is Induced by Dehydration

Next, we examined the expression of ET-3 during dehydration and found that the level of *ET-3* mRNA in the SFO increased

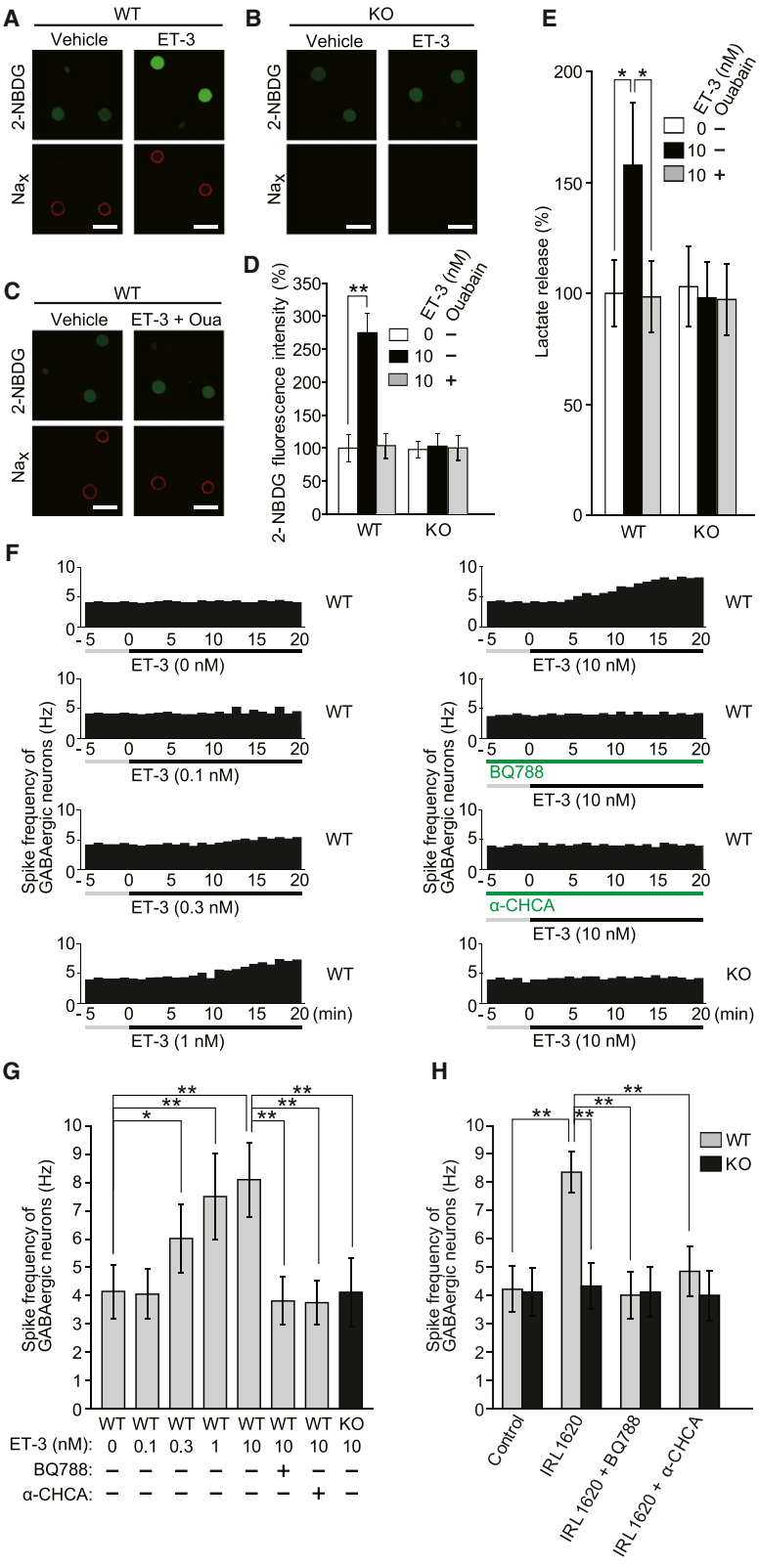

Figure 5. ET_BR Activation Causes Enhancement of Glucose Uptake and Lactate Release in Na_x-Positive Glial Cells and Leads to an Increase in the Firing Activity of GABAergic Neurons in the SFO

(A–C) Glucose imaging of dissociated SFO cells from WT (A, C) and *Na_x*-KO (B) mice 20 min after the application of vehicle or 1 nM ET-3 in a 140 mM Na^+ solution. To inhibit the activity of Na^+/K^+-ATPase, 1 mM ouabain was added to the extracellular solution (C). After the imaging, cells were stained with the anti-Na_x channel antibody (Na_x; red). Scale bars, 30 μm.

(D) Summary of glucose imaging of the SFO cells. Data were obtained from Na_x-positive cells. The mean fluorescence intensity in WT mice given vehicle was set at 100%. $^{**}p < 0.01$, two-tailed Student's t test; data are mean ±SEM (n = 20 for each).

(E) Lactate release from the SFO tissue into the incubation medium. SFO tissues from WT or *Na_x*-KO (KO) mice were incubated for 24 hr at 37°C, and the medium was subjected to measurements. Ouabain was added at 1 mM. $^{*}p < 0.05$, two-tailed Student's t test; data are mean ±SEM (n = 6 for each).

(F) Time course of the firing frequency in GABAergic neurons in the SFO tissues from *GAD-EGFP/Na_x*-WT (WT) mice. SFO tissues were treated with ET-3 during the indicated period.

(G and H) Summary of the firing frequency of GABAergic neurons in the SFO of *GAD-EGFP/Na_x*-WT (WT) and *GAD-EGFP/Na_x*-KO (KO) mice treated with ET-3 (G) or 100 nM IRL1620 (H). Average values of the firing frequency during 15–20 min were calculated. BQ788 and α-CHCA (an inhibitor of monocarboxylate transporters) was applied at 100 nM and 5 mM, respectively. $^{*}p < 0.05$, $^{**}p < 0.01$, two-tailed Student's t test; data are mean ±SEM (n = 8 for each). See also Figure S4.

time dependently (Figures 6A and 6B; approximately 10-fold at 36 hr as estimated from the signal intensity by in situ hybridization). On the other hand, ET_BR expression is not regulated by dehydration (in situ hybridization; data not shown), consistent with a previous finding obtained with a microarray (Hindmarch et al., 2008). The secreted ET-3 level in the SFO tissues was estimated by 1 hr incubation with different solutions (high Na^+, high osmolality, or high K^+) representing various conditions (Figure 6C). The ET-3 levels detected in the incubation solutions with the SFO from 48 hr dehydrated animals were all 6- to 8-fold larger than those from hydrated animals irrespective of the stimuli during the incubation, suggesting that ET-3 had been already secreted in the SFO tissues in vivo. As was expected, immunohistochemical analysis revealed that the phosphorylation of ERK1/2 was markedly enhanced in the SFO of dehydrated mice (Figure 6D).

Intriguingly, the specific upregulation of *ET-3* expression by dehydration was observed not only in WT mice but also in *Na_x*-KO mice (Figure 6E, WT and KO; estimated as 3.9 ± 0.7-fold by RT-PCR; n = 3), indicating that Na_x is not involved in this regulation. In contrast, the expression of ET-1 or ET-2 was not induced by dehydration (Figure 6E; see also Figure 1D). Of note, in vitro incubation of the SFO tissues from hydrated WT mice for 24 hr in a high Na^+ (170 mM $[Na^+]_o$) or hyperosmotic (350 mOsm; adjusted with mannitol) solution did not enhance the expression of ET-3 in the SFO (by in situ hybridization; data not shown),

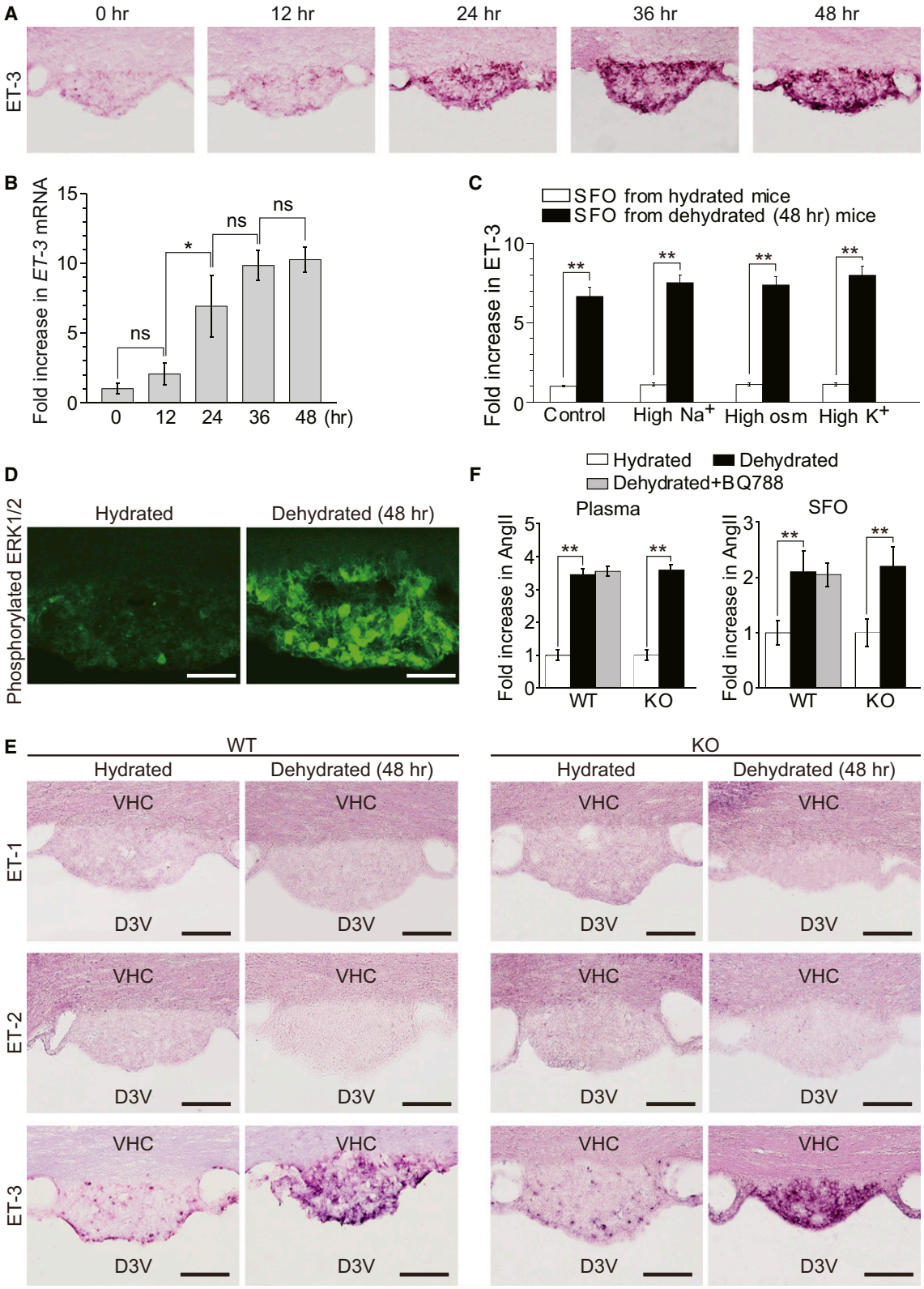

Figure 6. ET-3 Expression Is Enhanced by Dehydration

(A) In situ hybridization for detection of *ET-3* expression in the SFO of WT mice. Brains were obtained from mice provided freely with food and water (0 hr) or from those provided only with food during the indicated period (12, 24, 36, and 48 hr). In this experiment, specimen sets covering all conditions (0, 12, 24, 36, or 48 hr) were attached on the same glass slide for comparison. Sections on the same slide are shown.

(legend continued on next page)

suggesting that ET-3 expression is regulated by a signal from outside the SFO.

No Relation Was Detected between ET-3 Expression in the SFO and Ang II Expression

Ang II levels in blood and CSF increase under dehydrated conditions. Animals treated with Ang II increase their consumption of salt solutions in addition to water (Buggy and Fisher, 1974). We therefore examined the possibility that ET-3 and Ang II interact at some level. First, we investigated whether ET-3 or Na_x signaling regulates Ang II production. Ang II levels in blood and SFO showed a 2-fold increase at 48 hr dehydration (Figure 6F): The upregulation in the SFO is consistent with a previous report using rats (Barth and Gerstberger, 1999). Importantly, the levels did not differ between WT and *Na$_x$*-KO mice under hydrated or dehydrated conditions (Figure 6F), suggesting that Na_x signals are not involved in the regulation of Ang II production. *Na$_x$*-KO mice exhibit defects in salt-intake behavior, but not robust differences in water intake, blood pressure, or heart rate, under dehydrated conditions (data not shown). This also supports the view that Na_x signaling is not involved in the regulation of Ang II. In addition, Ang II levels in blood and SFO were not affected by the intracerebroventricular (i.c.v.) infusion of BQ788, which inhibits ET_BR (Figure 6F), indicating that ET-3 expression in the SFO is not relevant to Ang II production. Thus, it is unlikely that there is a direct relation between ET_BR (or Na_x) signaling and Ang II levels.

Next, we tested whether the renin-angiotensin system (RAS) is involved in the regulation of ET-3 expression. However, we could not obtain any data showing that Ang II is involved in the regulation of ET-3 in the SFO (Figure S5; see Supplemental Results).

ET_BR Antagonist Attenuates Salt Aversion in Dehydrated Mice through Modulation of the Gating Mechanism of Na_x

Finally, we verified the physiological significance of ET_BR activation to salt-intake behavior. We examined salt appetite using a two-bottle test in combination with the i.c.v. infusion of an ET_BR blocker, BQ788 (500 pmol/hr). Because the i.c.v. infusion of ET-3 significantly reduced the fluid intake of animals via unknown mechanisms (data not shown), we used a specific antagonist of ET_BR (BQ788) for this experiment. Continuous infusion of BQ788 or vehicle was performed for 2 days under hydrated and dehydrated conditions, and the amounts of 0.3 M NaCl and water taken in during the following 12 hr were measured (Figure 7A). Among WT mice in a hydrated condition, the preference ratio for the NaCl solution was slightly (not significantly) higher in the mice that received BQ788 (Figure 7B; WT, Hydrated). After dehydration for 1 and 2 days, the preference ratio for 0.3 M NaCl was markedly reduced in WT mice time dependently, but the reduction was significantly attenuated in the mice treated with BQ788 (Figure 7B; WT, Dehydrated). In contrast, in *Na$_x$*-KO mice, the preference ratio was not reduced by dehydration (Figure 7B; KO, Hydrated and Dehydrated). Moreover, it was not affected by the infusion by BQ788 in either the hydrated or dehydrated group (Figure 7B; KO, Hydrated and Dehydrated). These results suggest that ET_BR activation in the SFO enhances the sensitivity of the sodium sensor Na_x, thereby enhancing the salt-aversive behavior of the mice.

After dehydration, both WT and *Na$_x$*-KO mice showed a noted elevation in total fluid intake (Figure 7C) and a marked reduction in urine volume (Figure 7D) in the same way. In addition, urine $[Na^+]$ (Figure 7E) and serum $[Na^+]$ (Figure 7F) are slightly increased in both genotypes. These results are consistent with our previous reports (Watanabe et al., 2000; Hiyama et al., 2004; Nagakura et al., 2010). Of note, the i.c.v. infusion of BQ788 did not affect total fluid intake (Figure 7C), urine volume (Figure 7D), $[Na^+]$ in urine (Figure 7E), or $[Na^+]$ in serum (Figure 7F).

DISCUSSION

The concentration of Na^+ in serum is strictly controlled at 135–145 mM, and when over 145 mM results in a condition described as hypernatremia (Gladden, 2004). This means that the minimum threshold of the brain's $[Na^+]_o$ sensor for body-fluid homeostasis is lower than 145 mM in vivo under normal conditions. In the present study, we found that ET-3 is expressed in the SFO where Na_x is expressed and the sensitivity to $[Na^+]_o$ of Na_x depends on the concentration of ET-3; Na_x begins to open in the physiological $[Na^+]_o$ range when [ET-3] is more than 0.3 nM. We also found ET-3 expression to be commensurately enhanced in the SFO, according to the dehydration of animals. This improvement of the sensitivity of Na_x to $[Na^+]_o$ by ET-3 probably plays an essential role in keeping Na^+ concentrations in body fluids at normal levels by inducing salt aversion.

ET_BR is known to be expressed abundantly in the SFO as compared to ET_AR, though its physiological roles have not been elucidated (Hindmarch et al., 2008). In the present study, we revealed that ET-3 and ET_BR are coexpressed in Na_x-positive glial cells in the SFO, along with ET-converting enzymes (Figures 1A–1E). Importantly, ET-3 appears to be secreted in the SFO

(B) Changes in the signal intensity of the in situ hybridization for *ET-3* mRNA in the SFO during dehydration. Signal intensities are shown as relative values against that at 0 hr. *$p < 0.05$, two-tailed Student's t test; ns, not significant; data are mean ±SEM (n = 8 for each).
(C) Comparison of ET-3 levels secreted in SFO tissues of hydrated and 48 hr dehydrated mice. Five SFO tissue samples dissected from WT mice were collectively incubated with a certain amount of control solution ($[Na^+]_o$ = 145 mM), high-Na^+ solution ($[Na^+]_o$ = 170 mM), high-osmolality solution (osmolality = 350 mOsm), or high-K^+ solution ($[K^+]_o$ = 25 mM) for 1 hr at 37°C. The ET-3 concentrations are shown as relative values against that obtained from the SFO of hydrated mice under each condition. **$p < 0.01$, two-tailed Student's t test; data are mean ±SEM (n = 6 for each).
(D) Immunocytochemical detection of phosphorylated ERK1/2. The level of phosphorylated ERK1/2 in the SFO was increased by dehydration. Scale bars, 50 μm.
(E) In situ hybridization for detection of *ET-1*, *ET-2*, and *ET-3* expression in the SFO of the WT and *Na$_x$*-KO (KO) mouse brain. Brains were obtained from mice provided freely with food and water (Hydrated) or after 2 days without water (Dehydrated). The mRNA level of *ET-3*, but not *ET-1* or *-2*, was increased by dehydration. Scale bars, 100 μm.
(F) Comparison of Ang II levels in the plasma and SFO tissues of mice under hydrated or dehydrated (2 days) conditions. Ang II levels are shown as relative values against that of the hydrated WT mouse. Some mice were treated with BQ788 (500 pmol/hr) during the dehydration. **$p < 0.01$, two-tailed Student's t test; data are mean ±SEM (n = 6 for each). See also Figures S5 and S6.

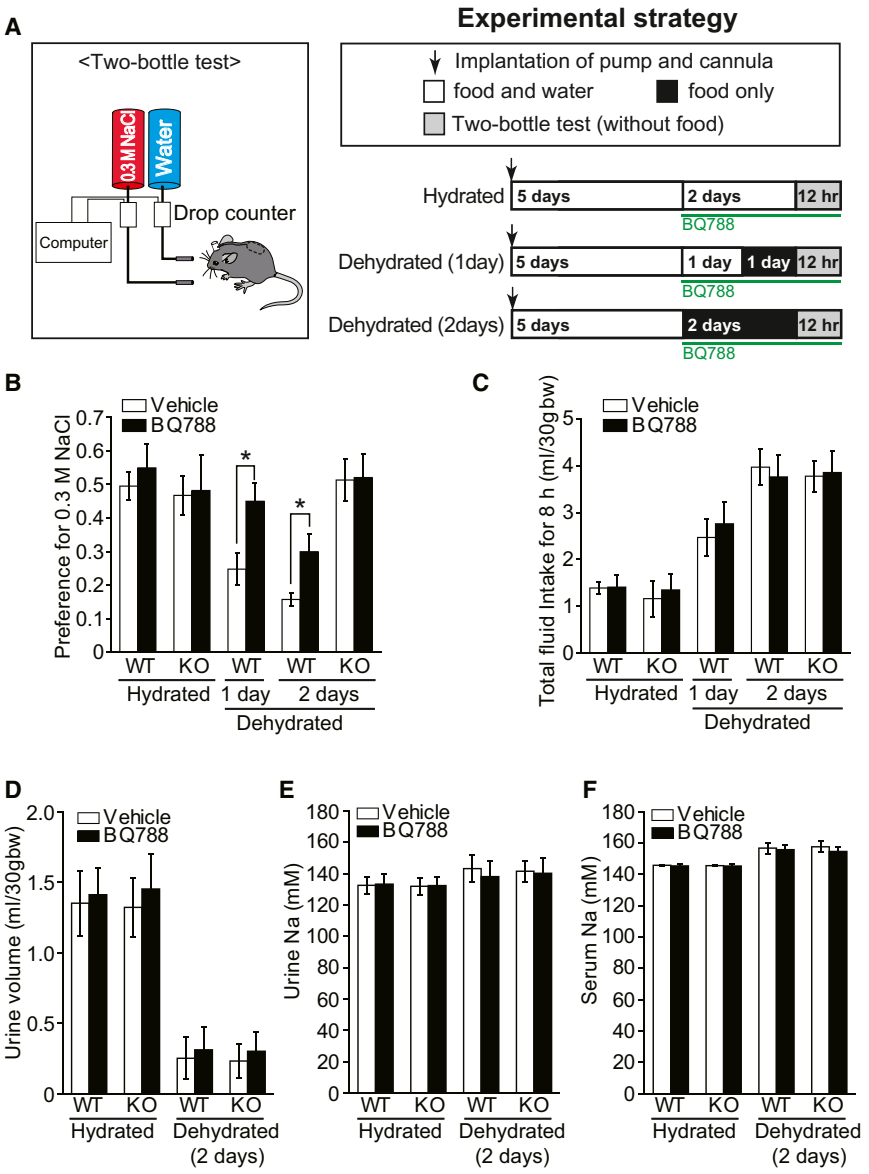

Figure 7. ET Signaling Is Involved in the Control of Salt-Intake Behavior in Mice

(A) Experimental design of the two-bottle test. After recovery from the implantation of an osmotic pump and cannula, the cannula was connected to the tube from the pump. Subsequently, the mice were housed with free access to water and food (Hydrated) or deprived of water (Dehydrated) for 1 or 2 days. Then the mice underwent the two-bottle test with 0.3 M NaCl and water. The mice received an i.c.v. infusion of BQ788 or vehicle during the period indicated with the bar underneath.

(B and C) Preference ratios for 0.3 M NaCl (B) and total intake volume (C) in the two-bottle test during 12 hr. WT and *Na*$_x$-KO (KO) mice received an i.c.v. infusion of BQ788 or vehicle were compared. The preference ratio was defined as the ratio of the volume of 0.3 M saline ingested to total fluid intake. *$p < 0.05$, two-tailed Student's t test; data are mean ±SEM (n = 10 for each).

(D and E) Urine volumes (D) and $[Na^+]$ (E) of the mice that received an i.c.v. infusion of BQ788 or vehicle. Urine samples were collected for 24 hr after the 2 day housing period indicated in (A). Data are mean ±SEM (n = 10 for each).

(F) Serum $[Na^+]$ of the mice that received an i.c.v. infusion of vehicle or BQ788 at the end of the 2 day housing period indicated in (A). Data are mean ±SEM (n = 10 for each).

(Figure 6C). Thus, ET-3 produced in the SFO likely activates ET_BR of Na_x-positive glial cells in an autocrine or paracrine fashion. As CVOs, including the SFO, lack a blood-brain barrier, cells in the SFO are supposedly exposed to circulating hormones, including ETs (Smith and Ferguson, 2010). However, ET-3 levels in plasma and CSF remained low during the 1–2 days of dehydration (ranged from 13 to 32 pM; see Supplemental Information). Because ET-3 at 50 pM did not affect Na_x gating (Figure 3E), ET-3 in blood or CSF is unlikely to activate Na_x channels in the SFO.

Importantly, 0.3 nM ET-3 is sufficient to partially activate Na_x channels under physiological conditions (Figures 1G, 1H, 2D, and 5G). Here, it should be noted that a certain amount of ET-3 is detected also under hydrated normal conditions (Figures 1D and 6A–6C). Based on the simple assumptions that ET-3 was distributed evenly in the SFO tissue and completely eluted out by incubation, the ET-3 level in the SFO after 48 hr dehydration was calculated to be ~1 nM (see Supplemental Information). Although it is difficult to estimate the local concentration of ET-3 in the SFO, even higher concentrations would be possible in vivo, because ET-3 is secreted into the intercellular space in the SFO; the space is very small, because processes of Na_x-positive glial cells tightly wrap the cell soma of neurons, including GABAergic neurons (Watanabe et al., 2006). These findings may suggest that the basic level of ET-3 already shifts the threshold of Na_x lower than 145 mM in vivo and that this modulation is essential for keeping Na^+ levels in body fluids in the physiological range. Enhancement of the sensitivity to $[Na^+]_o$ by ET_BR signaling probably brings about significant activation of Na_x even in slightly dehydrated animals through induction of ET-3 expression in the SFO, and this may help animals respond to dehydration steadily.

We demonstrated that Ang II does not induce Na^+ influx in Na_x-positive cells (Figures 1G, 1H, and S1A). Ang II is a vasoconstrictor peptide and promotes both water and salt intake (Paul et al., 2006; Fitzsimons, 1998). Its receptors are also abundant in the SFO, and the activation of Ang II receptors in the SFO reportedly stimulates salt intake (Fitzsimons, 1998). This is the opposite of Na_x activation, which leads to the suppression of salt intake (Noda, 2007). In addition, the data in Figures 6F and S5 demonstrate that it is unlikely that there is direct interaction between ET_BR (or Na_x) signaling and Ang II expression. Moreover, administration of BQ788 to hydrated animals did not affect

the stimulation of water or saline intake by i.c.v. injection of Ang II (data not shown), indicating that the effects of Ang II under hydrated conditions are independent of ET_BR signaling, probably because ET-3 expression is not enhanced. However, there remains the possibility that Na_x signaling regulates downstream of Ang II signaling in dehydrated animals (see below).

The fact that our baseline ingestion of salt is more than adequate for maintaining fluid balance indicates that salt-intake-promoting neurons are constitutively active at a certain level under normal conditions. Salt appetite is enhanced in hyponatremia and hypovolemia through induction of Ang II. On the other hand, inhibitory GABAergic neurons in the SFO, which probably suppress salt intake, also appear to be active at a certain level (they were firing at ~4 Hz under normal $[Na^+]$ conditions when analyzed ex vivo; Figure 5F; see also Shimizu et al., 2007). When $[Na^+]_o$ (or [ET-3]) was increased, the activity of SFO GABAergic neurons was upregulated by Na_x signaling (~8 Hz; Figure 5F; Shimizu et al., 2007); our data suggest that this enhancement of the inhibition is enough to suppress salt appetite (or to induce salt aversion). In *Na_x*-KO mice, this inhibition mechanism is deficient, and it is conceivable that they do not stop ingesting salt during dehydration. Thus, ET-3 is apparently implicated in the sensing mechanism of $[Na^+]$ in body fluids by Na_x, whereas Ang II is involved in the upregulation of salt/water-intake behaviors downstream. Salt intake would not be enhanced when the SFO GABAergic neurons are highly activated by Na_x signaling.

Neurons expressing Ang II receptors in the SFO appear to be composed of several distinct species that are involved in the stimulation of water intake, salt intake, vasopressin release, and so on. Among them, neurons relevant to the salt-intake regulation in the SFO presumably extend efferents to the bed nucleus of the stria terminalis and the central nucleus of the amygdala (Geerling and Loewy, 2008). As for the control mechanisms for salt intake by Na_x signaling, two possibilities are conceivable. One possibility is that SFO GABAergic neurons themselves project to these nuclei to control salt intake. Another is that Na_x signaling suppresses salt-intake-promoting projection neurons in the SFO via GABAergic neurons. Further studies, including the characterization of cell types and elucidation of local circuits in the SFO, would be required to understand the whole picture of brain mechanisms underlying salt homeostasis.

An important finding of the present study is that Na_x is not only $[Na^+]$-sensitive but also [ET-3]-sensitive; that is, Na_x has two synergistic activation mechanisms. Our in vitro experiments showed that Na_x is fully open at a $[Na^+]_o$ of 140 mM when [ET-3] is over 10 nM. Although it is not clear whether such conditions actually occur in vivo, other Na_x-positive cells might exist in which Na_x is activated solely by ET-3. Of note, Na_x is also expressed in some regions other than the SFO, including myometrium of the pregnant uterus, peripheral nonmyelinating Schwann cells, and pituicytes in the posterior pituitary (Watanabe et al., 2000, 2002). However, the physiological roles of Na_x in these areas have not been elucidated. Na_x is also expressed in alveolar type II cells in the lung, and the expression level is markedly enhanced just before and after birth in infants (Watanabe et al., 2002). We found that *ET-3* expression is also concomitantly induced in the lung at this developmental stage (Figure S6).

The finding that Na_x activation by ETs leads to the release of lactate from Na_x-positive glial cells suggests a possible distinct role for Na_x. At sites of brain damage, increases in extracellular lactate levels and activation of the uptake of lactate by neurons are observed (Chen et al., 2000; Mendelowitsch et al., 2001). In the CNS, we have observed that traumatic brain injury induces expression of Na_x in glial cells in damaged parts of the cortex (our unpublished observation). Moreover, it has been reported that ET_BR expression is also upregulated in glial cells after traumatic brain injury (Sirén et al., 2000) and ET-1 production increases in the damaged area (Petrov et al., 2002). Therefore, ETs may play an important role in the recovery from nerve injury by inducing the release of lactate from Na_x-positive cells.

In summary, this report demonstrates the existence of a dynamic mechanism—a change in the threshold of the $[Na^+]$ sensor for body fluids caused by the local expression of a vasorelaxation hormone, ET-3—in the SFO. This mechanism probably underlies the sensing of Na^+ concentrations in body fluids in vivo. ET_BR signaling subserves activation of Na_x channels and leads to the enhancement of glucose metabolism and lactate release in Na_x-bearing glial cells. This supply of lactate from glial cells eventually results in the activation of GABAergic neurons in the SFO. The activation of inhibitory neurons in the SFO is supposedly responsible for the negative control of salt appetite. Our findings thus provide insights into not only the gating mechanism of Na_x channels but also the physiological role of ET-3 in the SFO for salt homeostasis through neural control by glial cells.

EXPERIMENTAL PROCEDURES

For a detailed description of the procedures and other methods used, see Supplemental Information.

Experimental Animals

All experimental protocols with animals were reviewed and approved by The Institutional Animal Care and Use Committee of National Institutes of Natural Sciences, Japan (approval numbers 09A183, 10A236, 11A128, and 12A051). Male WT (C57BL/6J, CLEA Japan), homozygous *Na_x*-KO, heterozygous *GAD67-GFP* (Δneo) knockin (*GAD-GFP*), or *GAD-GFP* on the *Na_x*-KO genetic background (*GAD-GFP*/*Na_x*-KO) mice (Watanabe et al., 2006) at 8–12 weeks of age were used.

Intracellular Na^+ Imaging

Na^+ imaging was performed as described previously (Hiyama et al., 2010). Background fluorescence ratios of host cells without Na_x expression [Tet-off (−)] were subtracted from the respective values. For the curve fitting in Figure 3E, see Supplemental Experimental Procedures.

Patch-Clamp Experiments with Dissociated SFO Cells

For long-term recordings of whole-cell currents with better retention of intracellular constituents, the perforated patch method using β-escin was employed (Fan and Palade, 1998). The extracellular solution contained (in mM): 5 KCl, 2.5 $CaCl_2$, 1 $MgCl_2$, 20 HEPES, 10 NaOH, and appropriate amounts of NaCl (pH 7.4). Osmolality was adjusted to 350 mOsm with mannitol. The pipette solution contained (in mM): 120 Cs methanesulfonate, 20 TEA-Cl, 2 $MgCl_2$, 2 Na_2ATP, 1 EGTA, 10 HEPES, and 2 NaOH (pH 7.3). β-escin (30–50 μM) was added to the solution on the day of experiments, and osmolality was adjusted to 340 mOsm with mannitol. For the detection of Na^+-dependent currents, extracellular solutions were changed by the fast application method using a double-barreled application pipette (Johnson and Ascher, 1987). The pipette was operated by a piezoelectric device (PZ-150M, Burleigh Instruments).

Electrophysiology with SFO Slices

The electrophysiological experiments with the *GAD-GFP* and *GAD-GFP/Na_x*-KO mice were performed as reported elsewhere (Shimizu et al., 2007).

Estimation of ET-3 Levels in the SFO

To compare ET-3 secretion in various solutions, SFO tissues (n = 5) dissected from WT mice were collectively incubated with 100 μl modified Ringer solution (control solution; $[Na^+]_o$ = 145 mM), the solution with additional NaCl (high-Na^+ solution; $[Na^+]_o$ = 170 mM), the solution with additional mannitol (high-osmolality solution; osmolality = 350 mOsm), or the solution with additional KCl (high-K^+ solution; $[K^+]_o$ = 25 mM) for 1 hr at 37°C. Measurements were performed according to the manufacturer's instructions for the ET-3 radioimmunoassay kit (Bachem).

Intracerebroventricular Infusion

Mice were implanted with i.c.v. minipumps for chronic central infusion of the ET_BR-specific antagonist BQ788. Animals were allowed 5 days to recuperate. Subsequently, the cannula was connected to the pump with a polyethylene catheter to allow i.c.v. infusion of the drug. Osmotic minipumps (1002, alzet), which continuously deliver dissolved substances at a rate of 0.25 μl/hr, were filled with 2 mM BQ788 or vehicle (modified Ringer solution).

Two-Bottle Test

Two days after the start of the i.c.v. infusion, the ingested volume of distilled water or 0.3 M NaCl solution was measured for 12 hr. Preference in the two-bottle test was evaluated as a ratio of the volume of saline ingested to the total intake.

Statistical Analysis

Data were tested for statistical significance with Kyplot software (Kyens). $p < 0.05$ was considered statistically significant. Data are mean ±SEM.

SUPPLEMENTAL INFORMATION

Supplemental Information includes six figures, Supplemental Results, Supplemental Discussion, and Supplemental Experimental Procedures and can be found with this article online at http://dx.doi.org/10.1016/j.cmet.2013.02.018.

ACKNOWLEDGMENTS

GAD67-GFP mice were kindly provided by Y. Yanagawa (Gunma University, Japan). We thank T. Onaka (Jichi Medical University, Japan) for technical advice on the measurement of ET-3. We also thank N. Tomita, Y. Isoshima, and S. Miura for technical assistance and A. Kodama for secretarial assistance. This work was supported by grants-in-aid from the Ministry of Education, Culture, Sports, Science and Technology of Japan.

Received: September 24, 2012
Revised: January 9, 2013
Accepted: February 25, 2013
Published: March 28, 2013

REFERENCES

Arai, H., Hori, S., Aramori, I., Ohkubo, H., and Nakanishi, S. (1990). Cloning and expression of a cDNA encoding an endothelin receptor. Nature *348*, 730–732.

Barth, S.W., and Gerstberger, R. (1999). Differential regulation of angiotensinogen and AT_{1A} receptor mRNA within the rat subfornical organ during dehydration. Brain Res. Mol. Brain Res. *64*, 151–164.

Barth, S.W., Riediger, T., Lutz, T.A., and Rechkemmer, G. (2004). Peripheral amylin activates circumventricular organs expressing calcitonin receptor a/b subtypes and receptor-activity modifying proteins in the rat. Brain Res. *997*, 97–102.

Buggy, J., and Fisher, A.E. (1974). Evidence for a dual central role for angiotensin in water and sodium intake. Nature *250*, 733–735.

Chen, T., Qian, Y.Z., Rice, A., Zhu, J.P., Di, X., and Bullock, R. (2000). Brain lactate uptake increases at the site of impact after traumatic brain injury. Brain Res. *861*, 281–287.

Daniels, D., and Fluharty, S.J. (2004). Salt appetite: a neurohormonal viewpoint. Physiol. Behav. *81*, 319–337.

Fan, J.-S., and Palade, P. (1998). Perforated patch recording with β-escin. Pflugers Arch. *436*, 1021–1023.

Fitzsimons, J.T. (1998). Angiotensin, thirst, and sodium appetite. Physiol. Rev. *78*, 583–686.

Geerling, J.C., and Loewy, A.D. (2008). Central regulation of sodium appetite. Exp. Physiol. *93*, 177–209.

Gladden, L.B. (2004). Lactate metabolism: a new paradigm for the third millennium. J. Physiol. *558*, 5–30.

Goldin, A.L., Barchi, R.L., Caldwell, J.H., Hofmann, F., Howe, J.R., Hunter, J.C., Kallen, R.G., Mandel, G., Meisler, M.H., Netter, Y.B., et al. (2000). Nomenclature of voltage-gated sodium channels. Neuron *28*, 365–368.

Hindmarch, C., Fry, M., Yao, S.T., Smith, P.M., Murphy, D., and Ferguson, A.V. (2008). Microarray analysis of the transcriptome of the subfornical organ in the rat: regulation by fluid and food deprivation. Am. J. Physiol. Regul. Integr. Comp. Physiol. *295*, R1914–R1920.

Hiyama, T.Y., Watanabe, E., Ono, K., Inenaga, K., Tamkun, M.M., Yoshida, S., and Noda, M. (2002). Na_x channel involved in CNS sodium-level sensing. Nat. Neurosci. *5*, 511–512.

Hiyama, T.Y., Watanabe, E., Okado, H., and Noda, M. (2004). The subfornical organ is the primary locus of sodium-level sensing by Na_x sodium channels for the control of salt-intake behavior. J. Neurosci. *24*, 9276–9281.

Hiyama, T.Y., Matsuda, S., Fujikawa, A., Matsumoto, M., Watanabe, E., Kajiwara, H., Niimura, F., and Noda, M. (2010). Autoimmunity to the sodium-level sensor in the brain causes essential hypernatremia. Neuron *66*, 508–522.

Hori, S., Komatsu, Y., Shigemoto, R., Mizuno, N., and Nakanishi, S. (1992). Distinct tissue distribution and cellular localization of two messenger ribonucleic acids encoding different subtypes of rat endothelin receptors. Endocrinology *130*, 1885–1895.

Johnson, J.W., and Ascher, P. (1987). Glycine potentiates the NMDA response in cultured mouse brain neurons. Nature *325*, 529–531.

Kedzierski, R.M., and Yanagisawa, M. (2001). Endothelin system: the double-edged sword in health and disease. Annu. Rev. Pharmacol. Toxicol. *41*, 851–876.

Kohan, D.E., Rossi, N.F., Inscho, E.W., and Pollock, D.M. (2011). Regulation of blood pressure and salt homeostasis by endothelin. Physiol. Rev. *91*, 1–77.

Lin, M., Liu, S.J., and Lim, I.T. (2005). Disorders of water imbalance. Emerg. Med. Clin. North Am. *23*, 749–770, ix.

Mendelowitsch, A., Ritz, M.-F., Ros, J., Langemann, H., and Gratzl, O. (2001). 17β-Estradiol reduces cortical lesion size in the glutamate excitotoxicity model by enhancing extracellular lactate: a new neuroprotective pathway. Brain Res. *901*, 230–236.

Mendelsohn, F.A.O., Quirion, R., Saavedra, J.M., Aguilera, G., and Catt, K.J. (1984). Autoradiographic localization of angiotensin II receptors in rat brain. Proc. Natl. Acad. Sci. USA *81*, 1575–1579.

Nagakura, A., Hiyama, T.Y., and Noda, M. (2010). *Na_x*-deficient mice show normal vasopressin response to dehydration. Neurosci. Lett. *472*, 161–165.

Noda, M. (2006). The subfornical organ, a specialized sodium channel, and the sensing of sodium levels in the brain. Neuroscientist *12*, 80–91.

Noda, M. (2007). Hydromineral neuroendocrinology: mechanism of sensing sodium levels in the mammalian brain. Exp. Physiol. *92*, 513–522.

Paul, M., Poyan Mehr, A., and Kreutz, R. (2006). Physiology of local renin-angiotensin systems. Physiol. Rev. *86*, 747–803.

Peruzzo, M., Milani, G.P., Garzoni, L., Longoni, L., Simonetti, G.D., Bettinelli, A., Fossali, E.F., and Bianchetti, M.G. (2010). Body fluids and salt metabolism—part II. Ital. J. Pediatr. *36*, 78–85.

Petrov, T.H., Steiner, J., Braun, B., and Rafols, J.A. (2002). Sources of endothelin-1 in hippocampus and cortex following traumatic brain injury. Neuroscience *115*, 275–283.

Rauh, A., Windischhofer, W., Kovacevic, A., DeVaney, T., Huber, E., Semlitsch, M., Leis, H.-J., Sattler, W., and Malle, E. (2008). Endothelin (ET)-1 and ET-3 promote expression of *c-fos* and *c-jun* in human choriocarcinoma via ET_B receptor-mediated G_i- and G_q-pathways and MAP kinase activation. Br. J. Pharmacol. *154*, 13–24.

Robin, P., Boulven, I., Desmyter, C., Harbon, S., and Leiber, D. (2002). ET-1 stimulates ERK signaling pathway through sequential activation of PKC and Src in rat myometrial cells. Am. J. Physiol. Cell Physiol. *283*, C251–C260.

Saavedra, J.M., Correa, F.M.A., Plunkett, L.M., Israel, A., Kurihara, M., and Shigematsu, K. (1986). Binding of angiotensin and atrial natriuretic peptide in brain of hypertensive rats. Nature *320*, 758–760.

Sakurai, T., Yanagisawa, M., Takuwa, Y., Miyazaki, H., Kimura, S., Goto, K., and Masaki, T. (1990). Cloning of a cDNA encoding a non-isopeptide-selective subtype of the endothelin receptor. Nature *348*, 732–735.

Shimizu, H., Watanabe, E., Hiyama, T.Y., Nagakura, A., Fujikawa, A., Okado, H., Yanagawa, Y., Obata, K., and Noda, M. (2007). Glial Na_x channels control lactate signaling to neurons for brain [Na^+] sensing. Neuron *54*, 59–72.

Sirén, A.-L., Knerlich, F., Schilling, L., Kamrowski-Kruck, H., Hahn, A., and Ehrenreich, H. (2000). Differential glial and vascular expression of endothelins and their receptors in rat brain after neurotrauma. Neurochem. Res. *25*, 957–969.

Smith, P.M., and Ferguson, A.V. (2010). Circulating signals as critical regulators of autonomic state—central roles for the subfornical organ. Am. J. Physiol. Regul. Integr. Comp. Physiol. *299*, R405–R415.

Sokolovsky, M. (1995). Endothelin receptor subtypes and their role in transmembrane signaling mechanisms. Pharmacol. Ther. *68*, 435–471.

Watanabe, E., Fujikawa, A., Matsunaga, H., Yasoshima, Y., Sako, N., Yamamoto, T., Saegusa, C., and Noda, M. (2000). Na_v2/NaG channel is involved in control of salt-intake behavior in the CNS. J. Neurosci. *20*, 7743–7751.

Watanabe, E., Hiyama, T.Y., Kodama, R., and Noda, M. (2002). Na_X sodium channel is expressed in non-myelinating Schwann cells and alveolar type II cells in mice. Neurosci. Lett. *330*, 109–113.

Watanabe, E., Hiyama, T.Y., Shimizu, H., Kodama, R., Hayashi, N., Miyata, S., Yanagawa, Y., Obata, K., and Noda, M. (2006). Sodium-level-sensitive sodium channel Na_x is expressed in glial laminate processes in the sensory circumventricular organs. Am. J. Physiol. Regul. Integr. Comp. Physiol. *290*, R568–R576.